Seafloor Interaction with Steel Catenary Risers

by

Charles P. Aubeny, Giovanna Biscontin, & Jun Zhang
Texas A&M University

Final Project Report

Supported by Funding from:
Minerals Management Service
Under the MMS/OTRC Cooperative Research Agreement
1435-01-04-CA-35515
Task Order 35988
MMS Project Number 510

and

OTRC Industry Consortium

September 2006

OTRC Library Number: 9/06A173

For more information contact:

Offshore Technology Research Center
Texas A&M University
1200 Mariner Drive
College Station, Texas 77845-3400
(979) 845-6000

or

Offshore Technology Research Center
The University of Texas at Austin
1 University Station C3700
Austin, Texas 78712-0318
(512) 471-6989

A National Science Foundation Graduated Engineering Research Center

CONTENTS

1 Introduction 1

2 Equivalent Beam-Spring Model 2

3 Proposed *P-y* Model 6

3.1 Backbone Curve 7

3.2 Bounding Unload-Reload Loop 11

3.3 Reversals from and within the bounding loop 13

4 Input Parameters 16

5 Seafloor-Riser Interaction Model 19

6 Conclusions 20

7 Ongoing and Future Work 23

LIST OF FIGURES

1 Seafloor-Riser Interaction Problem. 1

2 Spring-Pipe Model. 3

3 Example riser deflection pattern in touchdown zone. 5

4 Typical *P-y* behavior. 5

5 Riser Trench and Seafloor Characteristics. 8

6 Backbone curves for rough riser pipes. 10

7 Backbone Curves for Smooth Riser Pipes. 10

8 Effect of Trench Width on Maximum Soil Resistance. 11

9 Bounding *P-y* loop. 12

10 Deflection reversals from the Bounding *P-y* Loop. 14

11 Deflection reversals from Arbitrary Point within the Bounding *P-y* Loop. 15

12 Measured *P-y* Loop after Dunlap et al. (1990) 17

13 Determination of Backbone Curve Coefficients, a and b. 17

14 Determination of Hyperbolic Curve Coefficients, k_o and ω. 18

15 Example of riser deflected shapes obtained from the program. 21

16 Example of predicted bending moment along the length of the riser 21

17 Schematic of the tests conducted by Bridge and Wiilis (2002) 22

18 Comparison of estimated and measured moments at gauge D. 22

LIST OF TABLES

1 Fitting coefficients for power law relationship between collapse load and cylinder embedment, $F/c_h D = a(h/D)^b$ for $0 \leq \eta \leq \infty$ 9

2 *P-y* Model Parameters Interpreted from Dunlap et al. (1990) data. 19

Abstract

The use of catenary steel compliant riser (SCR) systems has increased as hydrocarbon production has progressively moved further offshore and into deeper waters. The issue of fatigue damage caused by cyclic interaction of the riser with the seabed has gained prominence with the widespread use and lengthening of the spans. The problem involves a number of complex non-linear processes including trench formation, non-linear soil stiffness, soil suction, and breakaway of the riser from the seafloor. The analytical framework utilized in this research considers the riser-seafloor interaction problem in terms of a pipe resting on a bed of springs, the stiffness characteristics of which are described by non-linear load-deflection (*p*-*y*) curves. The *P*-*y* model allows for first penetration and uplift, as well as re-penetration and small range motions within the bounding loop defined by extreme loading. The backbone curve is constructed from knowledge of the soil strength, the rate of strength increase with depth, trench width and two additional parameters, while three parameters are necessary for the cyclic response.

1 Introduction

As hydrocarbon production progresses into deep and ultra-deep waters, conventional gravity systems are being replaced by compliant systems comprised of large floating systems attached to the seafloor by vertical tethers or mooring lines. The introduction of these compliant floating systems has led to the development of new designs for the riser pipes, with the catenary steel compliant riser (SCR) often being system of choice. Fatigue stresses associated with extreme storms, vessel movements, and vortex-induced vibrations are critical to SCR performance. The zone at which the SCR contacts the seabed, the touchdown zone (Figure 1), often proves to be a spot where bending stresses are largest and therefore a critical location for fatigue (Bridge et al., 2003, 2004). Analyses typically show fatigue damage to be sensitive to seafloor stiffness, which at present cannot be estimated with a great deal of reliability.

While linear elastic seafloor models (e.g., Pesce et al., 1998) provide very useful insights into seafloor-riser interactions, full-scale model tests (Bridge and Willis, 2002; Bridge et al., 2004) show that the riser problem involves complex non-linear processes including trench formation, non-linear soil stiffness, finite soil suction, and breakaway of the riser from the seafloor. This paper presents an analytical framework for soil-riser interaction based on a model comprising a linearly elastic pipe supported by non-linear springs. This model accounts for effects of initial

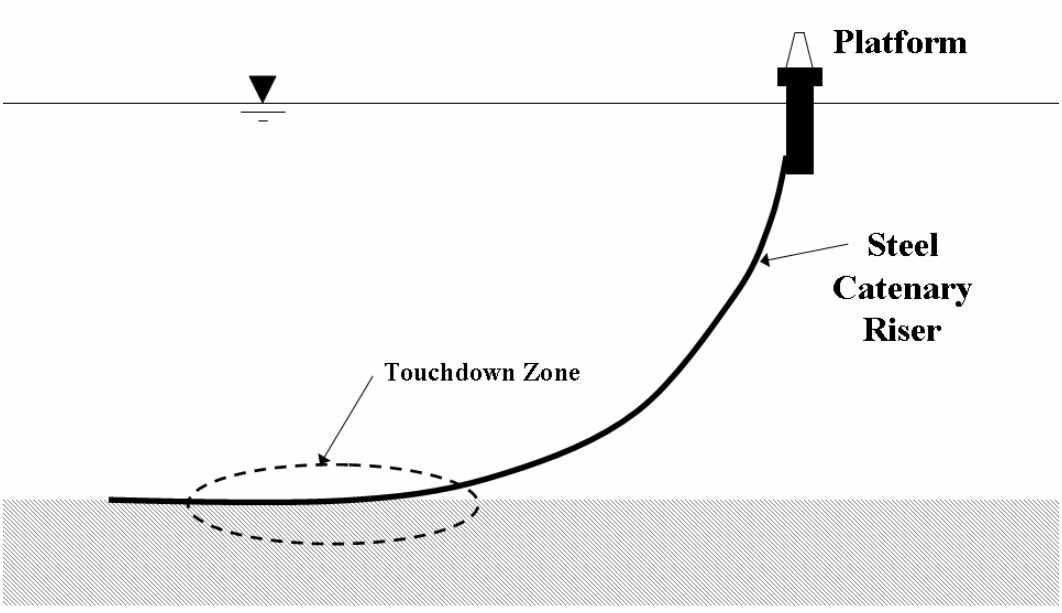

Figure 1: Seafloor-Riser Interaction Problem.

plastic penetration into the seafloor, non-linear soil stress-strain behavior, finite tensile strength of the seafloor and separation of the riser from the seafloor. Although lateral motions of the riser can affect riser performance (Morris et al., 1988; Hale et al., 1992), the current version of the model addresses only vertical riser motions. Observations indicate that riser trenches are typically about 4 pipe diameters wide. Hence, significant lateral soil resistance will only be mobilized for those displacement cycles large enough for the pipe to be pushed into contact with the walls of the trench. In contrast, vertical soil resistance will be mobilized during every load cycle, even small amplitude displacements. In addition, the magnitude of the soil resistance to vertical penetration is generally greater than that in the lateral direction due to the greater confinement (no nearby free surface) provided by the soil. The predominant trend in recently published literature, with regard to both model development (e.g., Bridge et al., 2004) and full-scale field tests (Bridge and Willis, 2002), is to focus on vertical motions. Given this situation, the primary focus of the work presented here was to develop, calibrate, and validate a vertical interaction model before addressing the secondary effects of lateral motions. Additionally, cyclic load tests of model pipes supported on soils (Dunlap et al., 1990; Clukey et al., 2005) indicate that soil stiffness degradation effects can be significant. The model presented herein does not simulate this behavior; however, incorporation of cyclic degradation effects is planned for future refinements of the model.

2 Equivalent Beam-Spring Model

The analytical framework utilized in this research considers the riser-seafloor interaction problem in terms of a pipe resting on a bed of springs (Figure 2), the stiffness characteristics of which are described by non-linear load-deflection (*P*-*y*) curves. The load term *P* designates the soil resistance in units of force per unit length in the horizontal (x) direction, and y refers to the vertical deflection of the riser pipe. The following non-linear, fourth-order ordinary differential equation governs this system:

$$EI\frac{d^4y}{dx^4} = W - P \tag{1}$$

where E, I and W are elastic modulus, moment of inertia, and weight per unit length of the riser pipe, respectively. The terms P and y are the soil resistance and deflection values computed in the current calculation step. Due to the non-linearity of the *P*-*y* relationship, the analysis procedure must iterate until the value of y assumed at the beginning of an iteration lies sufficiently close to

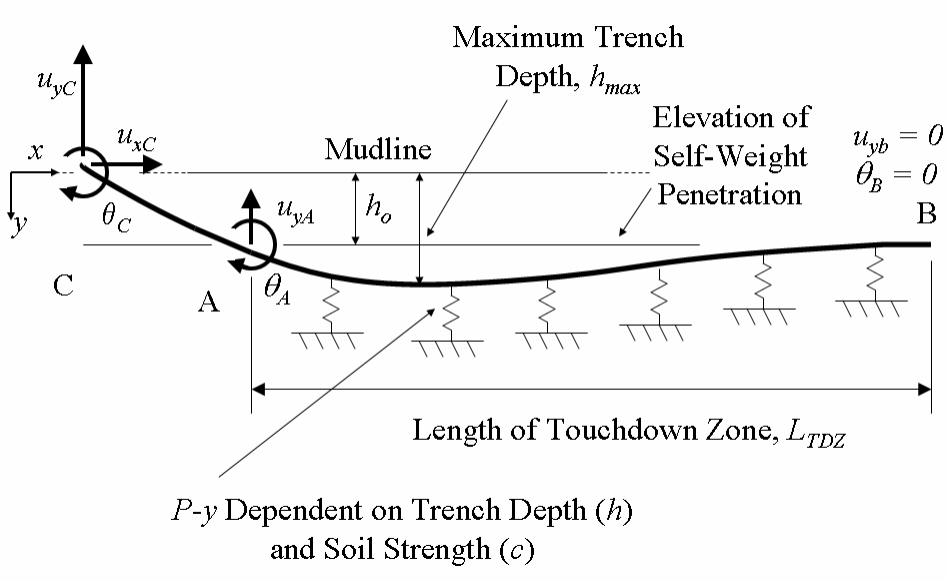

Figure 2: Spring-Pipe Model.

that computed from updated P and y values at the end of the iteration calculation.

It is noted that the complete riser problem, extending from the seafloor to the platform at the water surface, is inherently a large deformation problem. However, within the touchdown zone - the region of direct contact between seafloor and riser - lateral deflections on the order of 3 to 4 pipe diameters occur over a horizontal distance of several hundred diameters. This relative magnitude of lateral deflection is sufficiently small to justify the use of small-strain, small-deflection beam theory implicit in Eq. 1 when evaluating riser interaction effects within the touchdown zone.

Figure 2 illustrates the boundary conditions for the riser-seafloor interaction model. For planar motions an arbitrary point on the riser pipe (Fig. 2, Point C) has two displacement and one rotational degree of freedom, u_{xC}, u_{yC}, and θ_C, respectively. As the touchdown point (Fig. 2, Point A) is approached, the horizontal stiffness of the system is governed by the axial stiffness of an infinitely long pipe; i.e. for all practical purposes the system has infinite stiffness to the right of Point A and no horizontal deformations occur within the touchdown zone. Hence, conditions within the touchdown zone are modeled as a horizontal beam subjected to a time history of vertical displacements and rotations at the touchdown point u_{yA}, and θ_A. The remaining two boundary conditions necessary for solution of Eq. 1 are given by the far-field displacement constraints at Point B, u_{yB} = θ_B = 0. An additional requirement is that the shear and bending moment approach zero at Point B. This requirement is satisfied by making the length of the touchdown zone, L_{TDZ}, sufficiently large. The elevation of the riser pipe in the far field to the right of Point B will coincide with the

depth of riser pipe penetration due to its self-weight (h_o), which will not, in general, coincide with the mudline. Notice that the displacements boundary conditions shown in Figure 2 are referenced to the self-weight penetration depth; however, Eq. 1 is written in terms of the deflections from the mudline: $y = h_o - u_y$.

The authors recognize that certain large magnitude storm events may induce riser motions that are sufficiently large to translate the touchdown zone, either in the axial or lateral directions, to an entirely different location. This type of loading condition is not considered in the current model. The model discussed herein can accommodate localized separation of the riser pipe from the seafloor. However, the length of the zone of separation must be sufficiently small relative to the length of the touchdown zone such that the location of the far-field boundary (Fig. 2, Point B) need not be updated.

Solution of Eq. 1 is accomplished using a first-order central difference (Hornbeck, 1975) scheme. Figure 3 shows examples of typical computed riser configurations within the touchdown zone. The analysis proceeds through the following sequence:

1. computation of self-weight penetration of an undeformed pipe,
2. establishing an initial deformed configuration of the pipe,
3. applying a time history of successive motions (u_{yA},θ_A) to the pipe at the touchdown point.

The initial self-weight penetration calculation proceeds by simply equating pipe weight W to collapse load of a pipe embedded in a trench (details of the collapse load calculation will be discussed subsequently). In the case of this example, the pipe self-embedded about one pipe diameter. Estimating an initial riser configuration to initiate an analysis is a matter of some uncertainty at this point in time. However, existing observational data do provide a basis for establishing initial conditions. For example, observations have shown maximum riser pipe embedment within the touchdown zone to be in the range of about 3-4 pipe diameters (Willis and West, 2001; Thethi and Moros, 2001). Solution of Eq. 1 with an imposed contact angle θ_A at the touchdown point to achieve a target h_{max} appears to provide a reasonable basis for establishing an initial riser configuration. For the example simulation in question (Fig. 3), a rotation θ_A = 0.15 radians produced a maximum pipe embedment of about 3 pipe diameters below the mudline, or about 2 diameters below the depth of self-weight penetration. For both the self-weight penetration and the initial pipe configuration calculations are based on a purely plastic model of soil resistance.

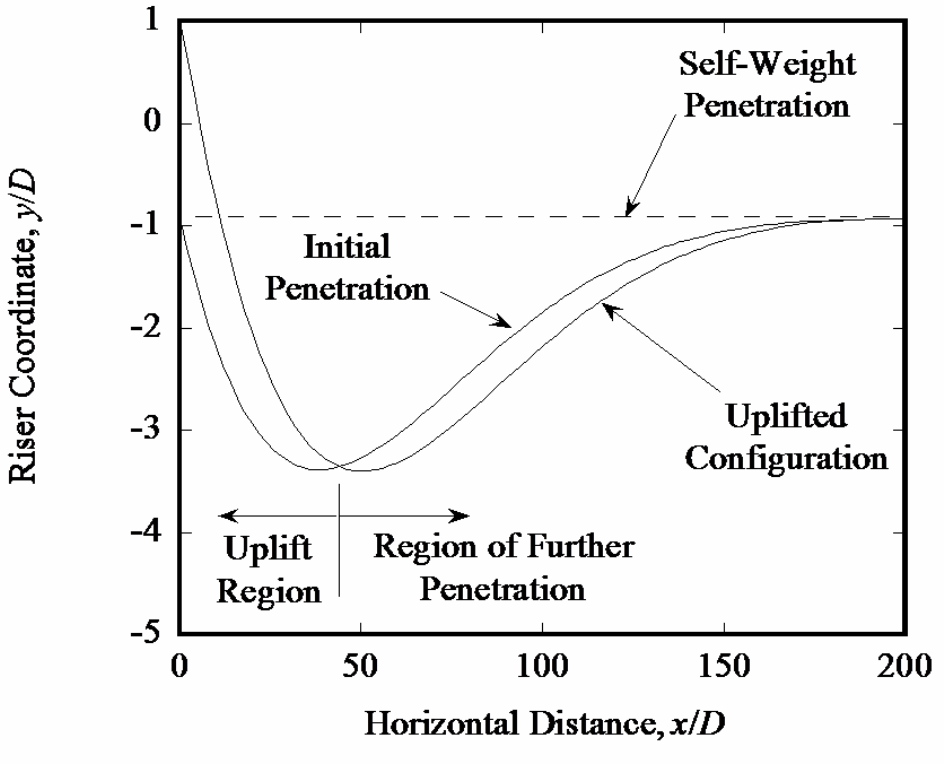

Figure 3: Example riser deflection pattern in touchdown zone.

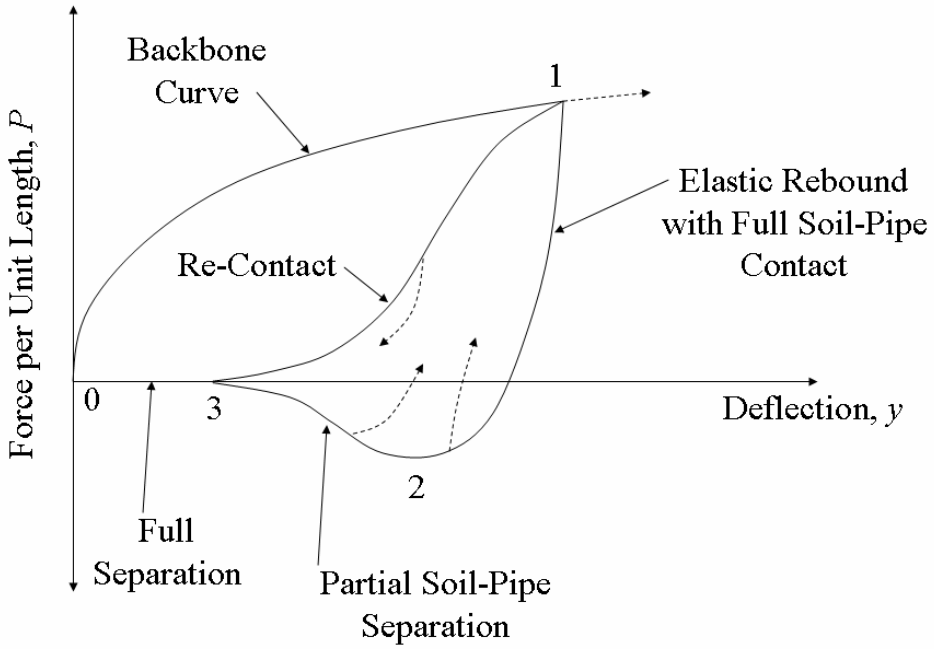

Figure 4: Typical *P*-*y* behavior.

The uplifted configuration shown in Figure 3 shows an example of the third step of the sequence described above, imposing subsequent motions to the initial configuration. In this example, a single uplift motion of two pipe diameters, $u_{yA} = 2D$, is imposed. The resulting computed pipe configuration shows a region extending about $x = 45D$ from the touchdown point in which uplifting of the pipe occurs. The seafloor-riser interaction in this region will be characterized by elastic rebound of the soil and, throughout much of this region, separation of the pipe from the seafloor. Beyond $x = 45D$ the direction of deflections reverses and continued plastic penetration into the seafloor occurs. Hence, even for the case of a simple uplift motion, the *P-y* model must be capable of describing a relatively complex pattern of behavior involving elastic rebound, seafloor-riser separation, highly variable magnitudes of deflection, reversal of deflection direction, and plastic penetration.

3 Proposed *P-y* Model

Laboratory model tests of vertically loaded horizontal pipes in weak sediment (Dunlap et al., 1990) produce the general load-deflection pattern shown in Figure 4. Path 0-1, referred to as a backbone curve, corresponds to virgin penetration of the riser into the seafloor. When a point on the riser experiences uplift, elastic rebound occurs and the *P-y* curve follows Path 1-2 in Figure 4. Previous studies (Dunlap et al., 1990; Bridge et al., 2004) indicate that appreciable soil suction may develop during uplift, although the maximum value of P in tension is significantly less than that in compression. At sufficiently large magnitudes of uplift motion, the pipe begins to separate from the seafloor, Point 2 in Figure 4. Model tests indicate that the breakaway is not abrupt; rather, the *P-y* curve gradually tends toward zero as depicted by Path 2-3 in Figure 4. With continued uplift the riser pipe is completely detached from the seafloor. Upon deflection reversal, the pipe again moves downward and eventually re-contacts the seafloor at Point 3 in Figure 4. Previous data (Dunlap et al., 1990; Bridge et al., 2004) also show that soil resistance does not mobilize abruptly upon re-contact between seafloor and riser; instead, soil resistance mobilizes gradually as depicted by the S-shaped Path 3-1 in Figure 4. Depending on the time history of motions imposed on the riser, further deflections can either involve repeated uplift along Path 1-2 or further deepening of the riser trench along Path 1-1' in Figure 4.

The preceding paragraph describes *P-y* behavior at a point along the riser pipe that experiences extremes of motion to the extent that full seafloor-riser separation occurs during an uplift cycle. A glance at the typical riser deflection patterns in Figure 3 clearly shows that such extremes of motion

do not occur at all points within the touchdown zone. In particular, deflection reversals can occur from any of Paths 1-2, 2-3, and 3-1 in Figure 4. Possible deflection reversal paths from intermediate points along the *P-y* loop are shown as dashed lines in Figure 4. Finally, further reversals can occur at any point along the dashed paths shown.

In view of the above discussion, a complete description of the *P-y* curve (Fig. 4) characterizing seafloor-riser interaction must include the following model components:

- Virgin penetration into the seafloor along Path 0-1-1'.
- A large deformation bounding loop (Path 1-2-3-1) encompassing elastic rebound with full seafloor-riser contact along Path 1-2, uplift with partial seafloor-riser separation Path 2-3 and re-contact and reloading along Path 3-1.
- Deflection reversal from any arbitrary point along the bounding loop.
- Load cycles within the bounding loop

The authors note that repeated load cycles will inevitably alter the characteristics of the *P-y* loop. The *P-y* model presented in this paper does not consider this effect, although this model is being formulated with a view toward accounting for cyclic loading effects in future refinements to the model.

3.1 Backbone Curve

The proposed model establishes the backbone curve based on collapse load computations for a horizontal cylinder (Fig. 5) of diameter D embedded in a trench of depth h. The collapse load P is related to soil strength c through a dimensionless bearing factor N_p as follows:

$$P = N_p c D \tag{2}$$

Early investigators on this topic includes Murff et al. (1989), who present collapse load estimates for horizontal cylinders embedded to a depth of up to $D/2$. Aubeny et al. (2005) extended the solution to trench depths of up to h = 5D and present collapse load estimates for non-uniform undrained shear strength profiles of the form:

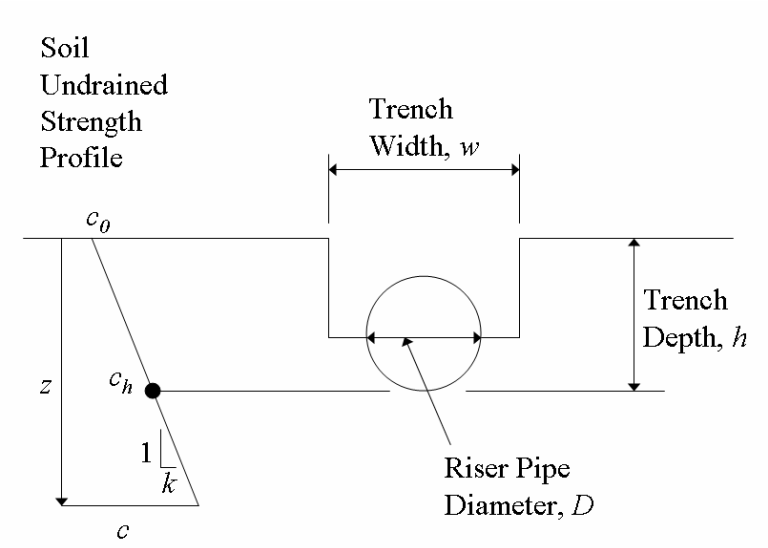

Figure 5: Riser Trench and Seafloor Characteristics.

$$c = c_o + k_z \tag{3}$$

where c_o is shear strength at the mudline and k is strength gradient with respect to depth z. Strength variability in the soil profile can be characterized in terms of a dimensionless parameter $\eta = k_D/c_o$. Based on finite element and method of characteristics solutions, Aubeny et al. (2005) found that, the bearing factor N_p is insensitive to variations in provided that the shear strength at the base of the trench, c_h (Fig. 6), is used as the reference strength in Eq. 2. They further found that, for trench width w/D = 1, an empirical power law function can effectively relate bearing factor N_p to trench depth h for general conditions of η as follows:

$$N_p = a(h/D)^b \tag{4}$$

Table 1 shows values fitting constants a and b for various conditions of penetration and pipe roughness.

Eq. 4 and Table 1 consider only cases where the trench width equals trench diameter, w/D = 1. Since visual observations indicate that the width of a trench formed by a riser pipe can be substantially greater than one pipe diameter, the present study extended the finite element collapse load calculations to trench width-to-depth ratios w/D = 2. Figs. 6 and 7 summarize the calculations. The studies showed that the effect of a widened trench is a reduction in the maximum bearing resis-

Boundary Roughness	Coefficients a, b	
	$h/D < 0.5$	$h/D < 0.5$
Smooth	a = 4.97 b = 0.23	a = 4.88 b = 0.21
Rough	a = 6.73 b = 0.29	a = 6.15 b = 0.15

Table 1: Fitting coefficients for power law relationship between collapse load and cylinder embedment, $F/c_h D = a(h/D)^b$ for $0 \leq \eta \leq \infty$.

tance, N_{pmax}, that develops at large h/D. Figure 8 illustrates the degree of the reduction in N_{pmax} with increasing w/D. Further, at sufficiently large w/D the collapse load behavior essentially follows that of a shallowly embedded pipe on a level ground surface; i.e., the shearing resistance from the soil mass adjacent to the side walls of the trench becomes negligible. Based on the finite element calculations, the trench width at which side wall resistance effects become negligible (Fig. 8) is about w/D = 2.75 for rough pipes and w/D = 2 for smooth pipes. Hence, N_p values predicted from Eq. 4 are capped to account for trench width effects according to the following relationships:

$$\text{Rough Pipes:} \quad N_{p\,max} = 7.74 - 1.22(w/D - 1) \qquad w/D < 2.75 \tag{5}$$

$$N_{p\,max} = 5.60 \qquad w/D > 2.75 \tag{6}$$

$$\text{Smooth Pipes:} \quad N_{p\,max} = 6.73 - 2.33(w/D - 1) \qquad w/D < 2 \tag{7}$$

$$N_{p\,max} = 4.40 \qquad w/D > 2 \tag{8}$$

In summary, critical characteristics of the backbone curve include riser pipe trench depth, trench width, and roughness at the soil-pipe interface. Increased trench depth h leads to increased bearing resistance N_p and is often associated with increased soil strength c. The proposed model characterizes the former effect by using a depth-dependent bearing factor (Eq. 4). Supported by the findings of Aubeny et al. (2005), the model incorporates the effects of a linearly increasing strength profile by taking the soil strength at the base of the trench, c_h, as the reference strength in Eq. 4. A widened trench ($w/D > 1$) tends to decrease the maximum bearing resistance $N_{p\,max}$ that can develop against the pipe. Eqs. 5 approximately characterizes this trench width effect. The model utilizes the relationships in Eqs. 5 to cap N_p values from Eq. 4. Fitting parameters in Eqs. 4 and 5 have been developed for two limiting conditions of pipe roughness: completely rough with no slippage occurring at the soil-riser interface and completely smooth with full slippage at the in-

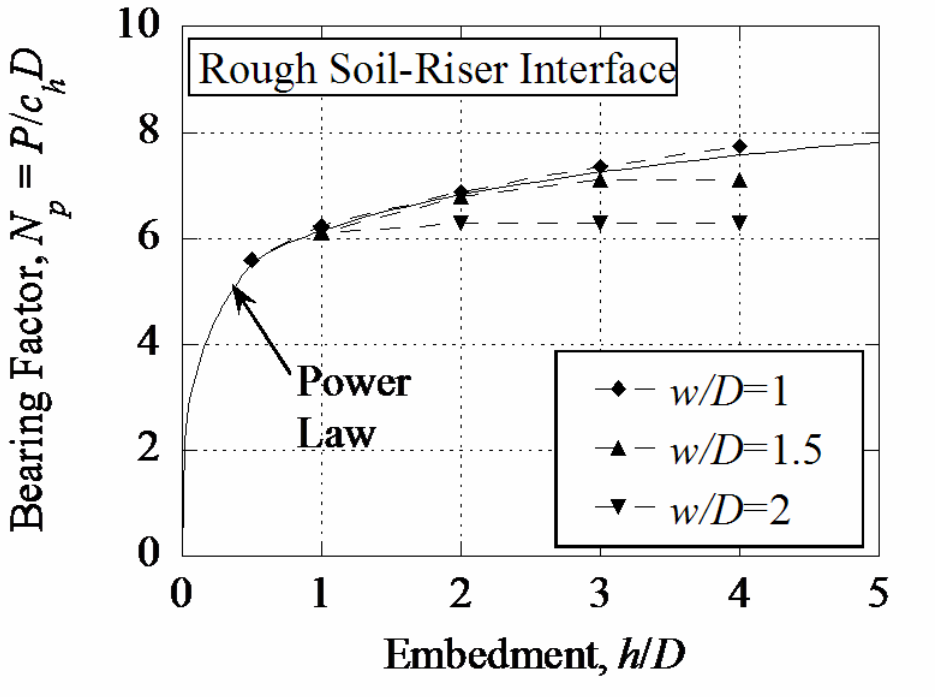

Figure 6: Backbone curves for rough riser pipes.

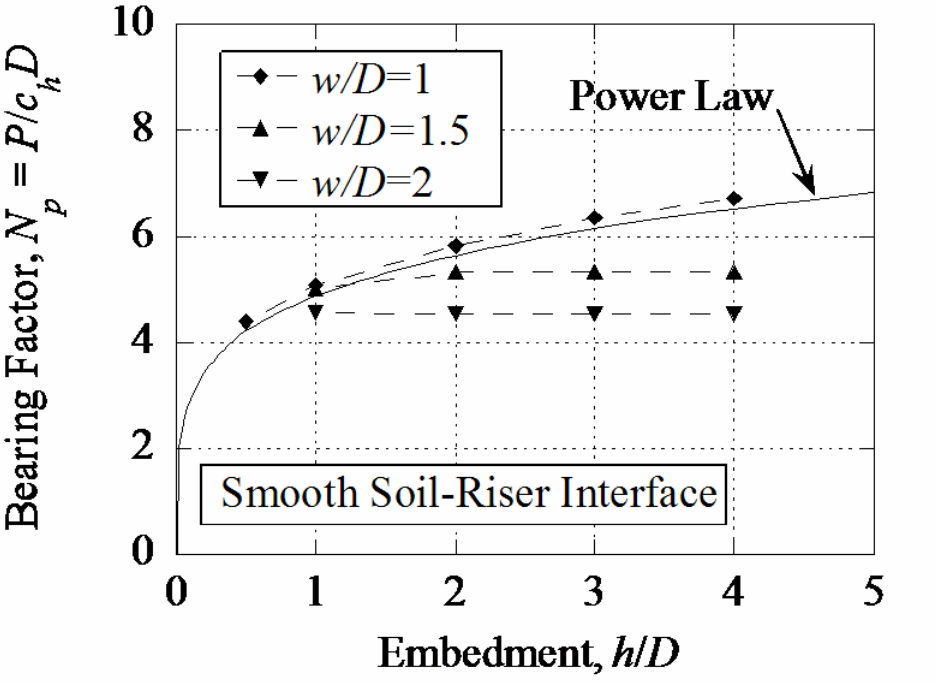

Figure 7: Backbone Curves for Smooth Riser Pipes.

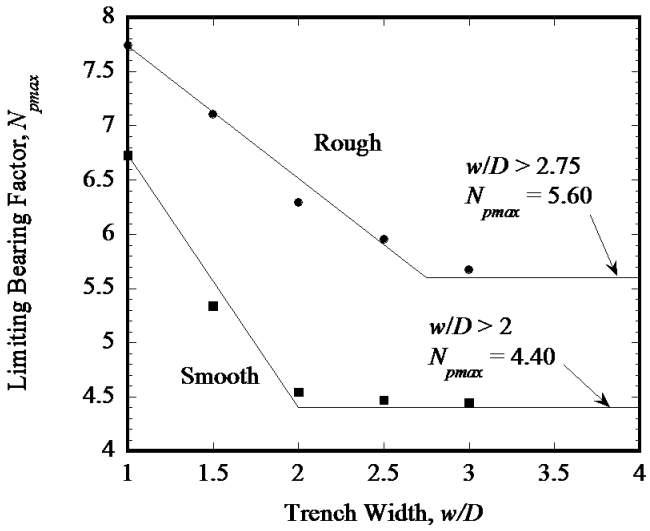

Figure 8: Effect of Trench Width on Maximum Soil Resistance.

terface. Intermediate roughness conditions are approximated by linear interpolation between these two extremes. Finally, it should be noted that the trench width w is not likely to be uniform along the entire length of the touchdown zone. For example, w is likely to be large at the touchdown point (Point A in Fig. 2) where lateral riser motions are greatest, and narrower at other locations. The form of Eqs. 5 permits adjustment of $N_{p\,max}$ for continuous variations in w.

3.2 Bounding Unload-Reload Loop

As noted earlier, upon experiencing a sufficiently large unload-reloading cycle from the backbone curve, the *P-y* curve will following a 'bounding loop' characterized by a sequence of elastic rebound, partial and full separation of riser from seafloor, and re-contact and re-loading. To simulate this process, the proposed model employs a mathematical formulation with the following features:

- The geometry of the loop is described in terms of three fixed points in *P-y* space (Fig. 9). Point 1 (P_1, y_1) is the point on the backbone curve from which the unload-reload cycle is initiated. Point 2 (P_2, y_2) is the point at which the maximum level of tension (suction) is mobilized during uplift. Point 3 (P_3, y_3) is the point at which the riser pipe becomes completely detached from the seafloor.

- Point 1 is a state variable determined by the maximum previous plastic penetration of the

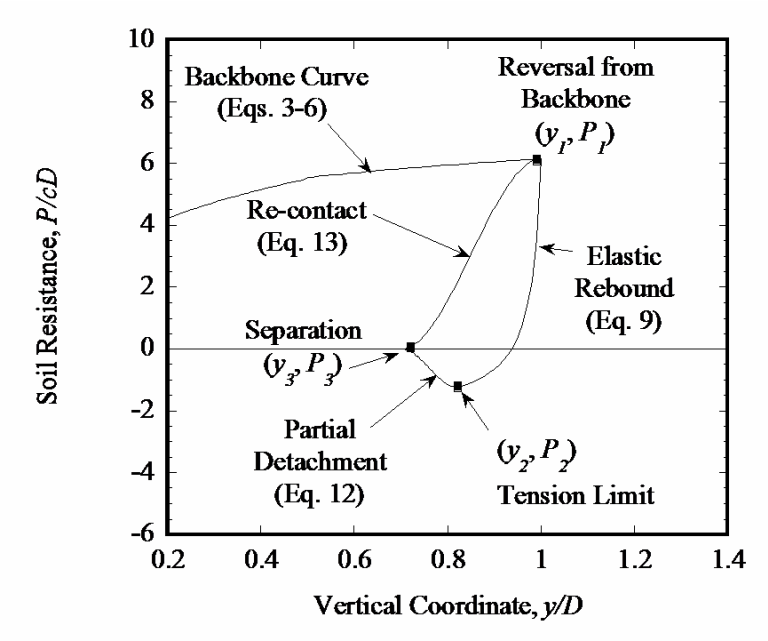

Figure 9: Bounding *P*-*y* loop.

riser into the seafloor. Point 2 is established using a model parameter relating maximum tension to maximum compression:

$$P_2 = -\phi P_1 \tag{9}$$

Point 3 is established using a model parameter relating the deflection interval over which detachment of the riser occurs to the deflection interval between Points 1 and 2:

$$(y_2 - y_3) = \psi(y_1 - y_2) \tag{10}$$

- A hyperbolic relationship defines the elastic rebound *P*-*y* curve between Points 1 and 2 as follows:

$$P = P_1 + \frac{y - y_1}{\frac{1}{k_o} + \chi\frac{y-y_1}{(1+\omega)P_1}} \tag{11}$$

The parameter k_o defines the initial slope of the hyperbola and controls the asymptote of the hyperbola. The parameter χ is simply a positive or negative sign according to whether loading or unloading occurs. For the case of unloading under discussion, χ = -1. The parameter k_o is ideally estimated from laboratory model test measurements. Absent such data, finite element studies indicate that k_o relates to soil undrained elastic modulus E_u as follows:

$$k_o \approx 2.5E_u \tag{12}$$

Finite element studies also show that the constant relating E_u to k_o in Eq. 12 is relatively insensitive to conditions of trench depth or width.

The tension limit imposed by Eq. 9 truncates the hyperbola at Point 2 such that:

$$y_2 = y_1 - \frac{(1+\omega)P_1}{k_o}\frac{1+\phi}{\omega-\phi} \tag{13}$$

Figure 9 shows an example of a hyperbolic elastic rebound curve between Points 1 and 2.

- A cubic relationship defines the *P-y* curve in the seafloor-riser zone between Points 2 and 3 as follows:

$$P = \frac{P_2}{2} + \frac{P_2}{4}\left[3\left(\frac{y-y_0}{y_m}\right) - \left(\frac{y-y_0}{y_m}\right)^3\right] \tag{14}$$

$$y_0 = \frac{y_2+y_3}{2} \tag{15}$$

$$y_m = \frac{y_2-y_3}{2} \tag{16}$$

A similar cubic relationship defines the *P-y* curve in the re-contact/reload zone between Points 3 and 1:

$$P = \frac{P_1}{2} + \frac{P_1}{4}\left[3\left(\frac{y-y_0}{y_m}\right) - \left(\frac{y-y_0}{y_m}\right)^3\right] \tag{17}$$

$$y_0 = \frac{y_1+y_3}{2} \tag{18}$$

$$y_m = \frac{y_1-y_3}{2} \tag{19}$$

Figure 9 shows examples of cubic functions describing the *P-y* curve in the regions of partial separation during uplift (Eq. 14) and re-contact during reloading (Eq. 17).

3.3 Reversals from and within the bounding loop

The discussion in the preceding paragraphs considers *P-y* relationships under conditions of extreme displacement; i.e., deflection reversal from the maximum penetration depth Points 1 and deflection

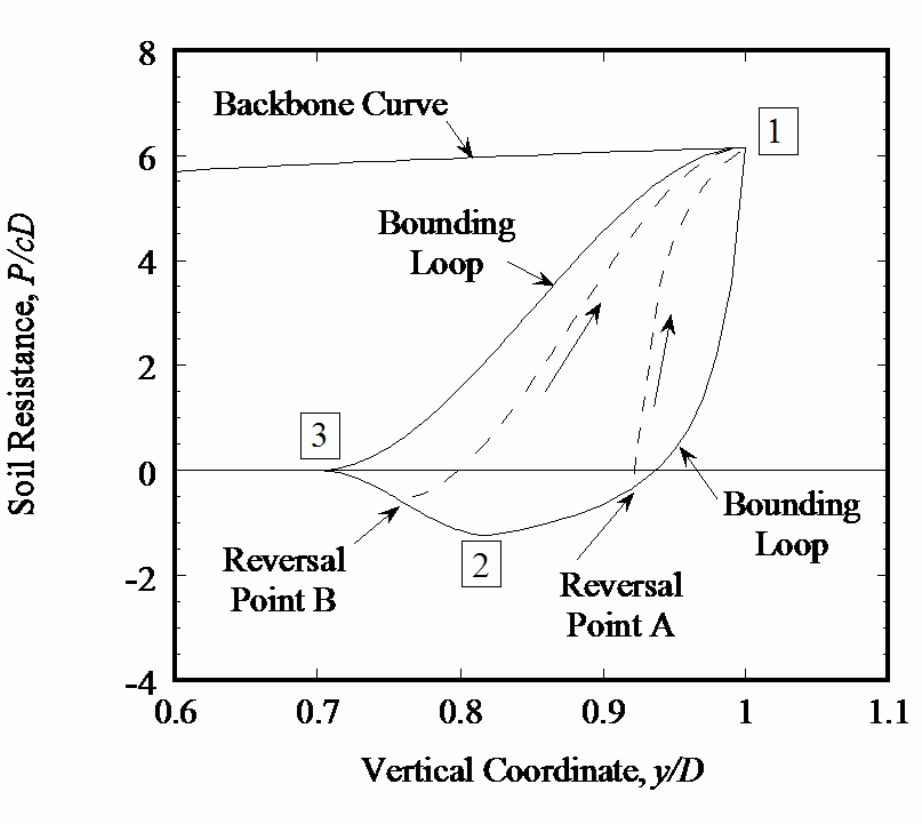

Figure 10: Deflection reversals from the Bounding *P*-*y* Loop.

reversal from the point of incipient contact, Point 3. In general, deflection reversals can occur from any point along the bounding loop from an arbitrary reversal point on the bounding loop (P_{rB}, y_{rB}). Deflection reversals from bounding loop segments 1-2 (elastic rebound) and 3-1 (re-contact) are modeled using a modified form of Eq. 11, with an arbitrary reversal point (P_{rB}, y_{rB}) replacing (P_1, y_1):

$$P = P_{rb} + \frac{y - y_{rb}}{\frac{1}{k_o} + \chi \frac{y - y_{rb}}{(1+\omega)P_1}} \tag{20}$$

As noted earlier, for reloading χ = 1 and for unloading χ = -1. For sufficiently large levels of deflection reversal, $y - y_r$, the *P*-*y* curve defined by Eq. 20 can intersect the bounding loop. At this point, the governing *P*-*y* equation reverts to the appropriate bounding loop equation, Eq. 2 or Eq. 14. Figure 10 shows an example of deflection reversals from segment 1-2 of the bounding loop, with a hyperbolic load path departing from reversal point A.

Deflection reversal from bounding loop segment 2-3, the region of partial detachment, follows a

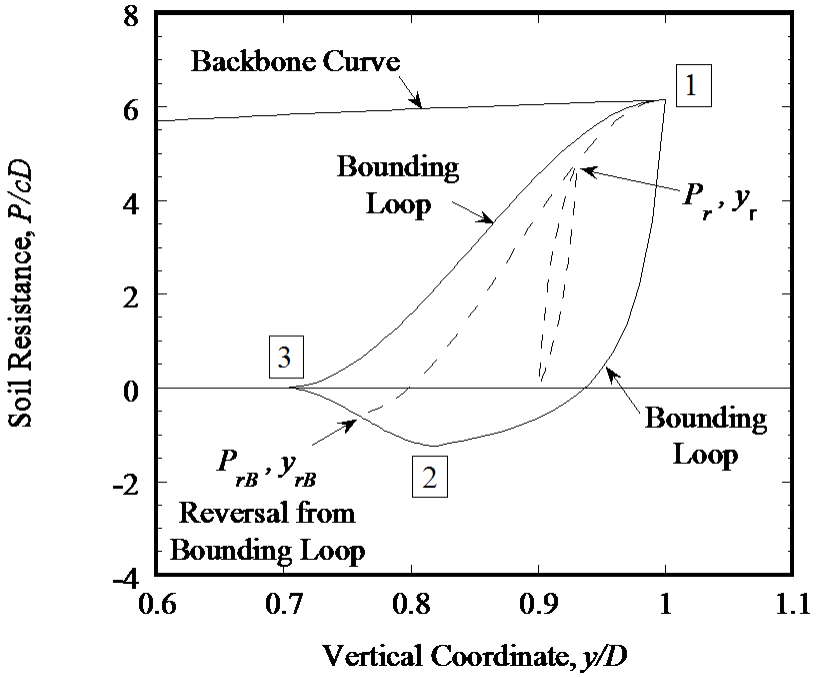

Figure 11: Deflection reversals from Arbitrary Point within the Bounding *P-y* Loop.

modified form of Eqs. 17:

$$P = \frac{P_{rb} + P_1}{2} + \frac{P_1 - P_{rb}}{4} \quad 3 \quad \frac{y - y_0}{y_m} \quad - \quad \frac{y - y_0}{y_m} \quad ^3 \tag{21}$$

$$y_0 = \frac{y_1 + y_{rb}}{2} \tag{22}$$

$$y_m = \frac{y_1 - y_{rb}}{2} \tag{23}$$

Figure 10 shows an example of a deflection reversal from segment 2-3 of the bounding loop, with a cubic load path departing from reversal point B.

Finally, rules are required for defining *P-y* behavior for a deflection reversal for any arbitrary reversal point (P_r, y_r) from a path prescribed by either Eq. 20 or 21. The reversals are always governed by Eq. 17, except that (P_r, y_r) is used in lieu of (P_{rb}, y_{rb}). Figure 11 shows an unload-reload loading loop starting from a point (P_r, y_r) that does not lie on the bounding loop.

In summary, the *P-y* behavior at any arbitrary location on or within the bounding loop is a path-dependent process. Description of the path requires load direction parameter χ and following state

variables:

- The point of maximum advancement on the backbone curve, Point 1 (P_1, y_1).
- The point of the last deflection reversal from the bounding loop (P_{rb}, y_{rb}).
- The point of the last deflection reversal (P_r, y_r)

4 Input Parameters

A complete implementation of Eq. 1 requires a series of model parameters that include three riser pipe properties, two soil parameters, one trench geometry parameter, two backbone curve model parameters, and four bounding loop model parameters. The three riser pipe properties - the elastic modulus of the pipe E, moment of inertia I, and weight per unit length W - are well-defined material and geometric parameters that involve little uncertainty with regard to model implementation. The two soil parameters - mudline strength c_o and strength gradient k - exert a crucial influence on soil stiffness (see Eqs. 2 and 3); however, evaluation of the soil strength parameters does not require techniques unique to the proposed model. Rather, the soil strength parameters, c and k, can be evaluated using proven site investigation tools, such as the cone penetration test or the T-bar (Stewart and Randolph, 1994). Given that the soil depth of interest is quite shallow, impact penetration tests (Aubeny and Shi, 2006) may also prove useful for this purpose. The single trench geometry parameter, width w (Eq. 5), should perhaps more aptly be considered as a function of location, $w(x)$. The proposed model does not predict trench width, and the authors envision using direct physical observations of trench geometry as a basis of estimating $w(x)$.

The backbone curve and bounding loop parameters utilized in the model in general require special laboratory tests involving instrumented pipes penetrating into a clay-filled test basin. Load-penetration measurements collected during initial penetration are utilized to determine the two backbone curve parameters, a and b in Eq. 4. Measurements collected during an unload cycle are utilized to determine the hyperbolic parameters k_o and ω in Eq. 11, the tension limit ϕ in Eq. 9, and the soil-riser separation parameter ψ in Eq. 10.

Figure 12 shows an example of such a test interpretation using the basin test data of Dunlap et al. (1990), which includes initial plastic pipe penetration to Point 1, followed by unloading to full separation between soil and pipe. The power law form of the backbone curve in Eq. 2 implies a linear relationship between initial penetration force and deflection during when plotted on a log-log

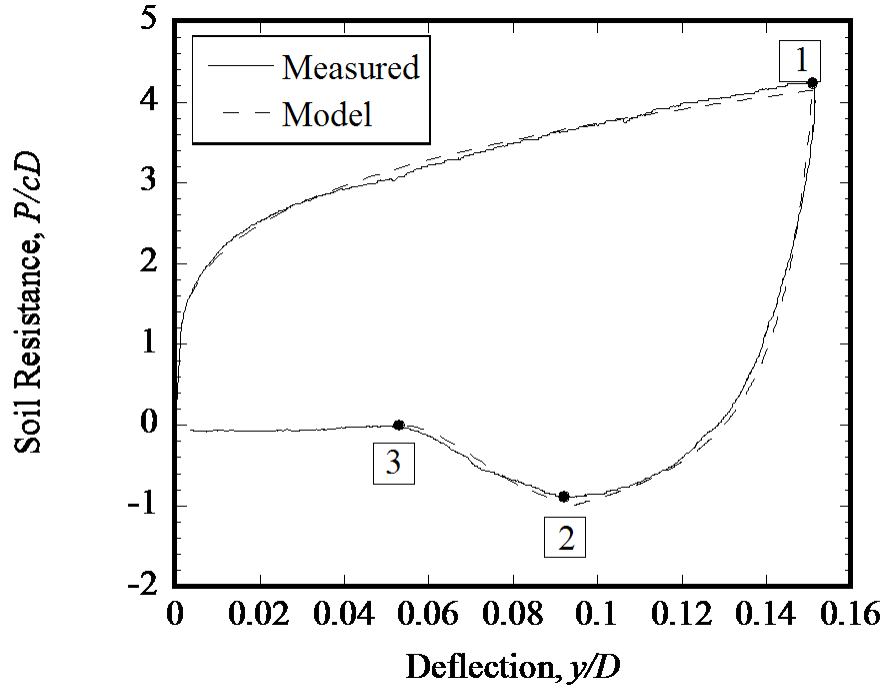

Figure 12: Measured *P-y* Loop after Dunlap et al. (1990)

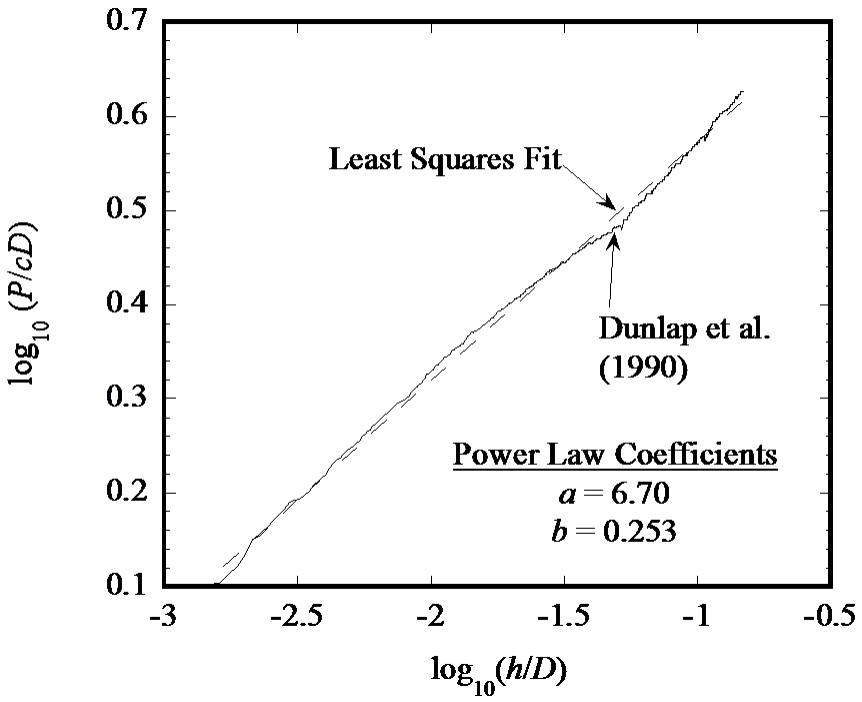

Figure 13: Determination of Backbone Curve Coefficients, a and b.

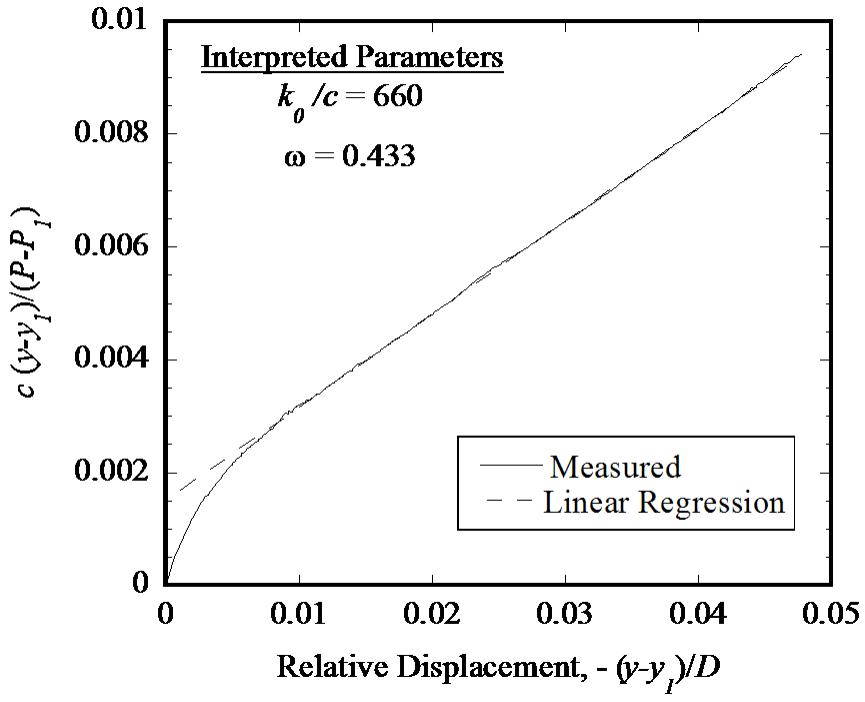

Figure 14: Determination of Hyperbolic Curve Coefficients, k_o and ω.

scale. Figure 14, showing such a log-log plot of initial penetration force-deflection measurements, in fact shows an essentially linear relationship, thus supporting the power law form of the backbone curve used in the model. Moreover, a simple linear regression analysis of the data in Figure 13 yields measured backbone curve coefficients a = 6.70 and b = 0.253. Comparison to the theoretical a and b values in Table 1 shows the measured values to be bracketed by the theoretical values for rough and smooth pipes.

When interpreting the hyperbolic portion of the unload curve between points 1 and 2, the data are most expeditiously interpreted by transforming Eq. 11 as shown in Figure 14:

$$\frac{y - y_1}{P - P_1} = \frac{1}{k_o} + \frac{\chi}{(1+\omega)P_1}(y - y_1) \tag{24}$$

As noted earlier, χ is simply a negative sign for unloading. When plotted in this manner, a hyperbolic load-deflection relationship will plot as a straight line with intercept $1/k_o$ and slope $1/(1+\omega)P_1$. Examination of Figure 14 shows that, except for very small deflections the measured data are almost perfectly linear, thus supporting the hyperbolic form of the load-deflection curve assumed in the model. In the linearized format of Eq. 24, the parameters k_o and are readily derived

Parameter	Description	Value
a	Backbone Curve Coefficient	6.70
b	Backbone Curve Exponent	0.254
k_o/c	Unload Initial Stiffness	660
ω	Unload Large Deflections	0.433
ϕ	Unload Tension Limit	0.203
ψ	Soil-Riser Separation	0.661

Table 2: *P-y* Model Parameters Interpreted from Dunlap et al. (1990) data.

from a simple linear regression analysis. Interpreted parameters are listed in Table 2. It should be noted that a direct determination of k_o based on the tangent of the load-deflection curve at small deflections will typically be sensitive to small errors in load or deflection measurements. Data interpretation using Eq. 24 avoids this potential problem.

Finally, the tension limit parameter ϕ and the soil-riser separation parameter ψ are determined directly from measured data using Eqs. 9 and 10, respectively. Interpreted parameters are listed in Table 2. Use of the model parameters tabulated in Table 2 with the corresponding constitutive equations yields the model simulation of the test designated as a dashed line in Figure 13. Comparison of measurements versus model simulation indicates that the proposed model is capable of realistically describing actual *P-y* behavior.

5 Seafloor-Riser Interaction Model

With *P-y* behavior characterizing soil resistance as described above, the analysis of soil-interaction interaction can proceed through finite difference solution of Eq. 1. Boundary constraints are as illustrated in Figure 2, with excitation in the form of imposed vertical displacements and rotations being applied at the touchdown point. The primary solution variable is vertical deflection y. Figure 15 illustrates typical profiles of deflection versus horizontal coordinate calculated from the program. From the standpoint of fatigue life, a primary consideration is bending moment. The analysis presented herein utilizes a first-order central difference formulation to second derivatives of y in the bending moment calculation. Figure 17 illustrates typical bending moment profiles. Evaluation and calibration of the seafloor-riser interaction model through comparisons to extant field data is the primary focus of the remaining research effort on this project.

The following discussion presents a preliminary presentation of this ongoing work. Bridge and Wiilis (2002) present some findings from a field test program involving a 360-ft long, 6-5/8 in diameter steel catenary riser field test. The riser pipe was instrumented at 13 locations as shown in Figure 17 to allow measurements of bending moments. An actuator induced vertical motions at the right end of the riser pipe, with the riser elevation at this point varying from 29 to 36.2 ft above the seabed. During the test program, a riser trench developed to a maximum depth of about 1.25 ft. The test was performed in a harbor subjected to tidal currents. Although the exact mechanism of trench formation has not fully been explained yet, combinations of riser motions and fluid flow were considered as major factors. The seabed consists of a high plasticity clay having an estimated undrained shear strength of 73 psf and a sensitivity of 3.3. The test program was part of a STRIDE JIP (Steel Risers in Deepwater Environments Joint Industry Project). Access to all test data is limited to the JIP ticketholders; however, some significant data have appeared in published literature. Figure 18 shows an example of the bending moment history at strain gauge location D during an initial pullout-laydown test. Location D is particularly interesting, since that point is initially in the touchdown zone. It is then lifted completely out of contact with the seafloor during the uplift cycle and set back onto the seafloor during the laydown cycle. Initial comparison of model predictions to measurements indicate that the model overestimates the magnitude of the change in the bending moments during the load cycle, but realistically simulates the distorted 'figure 8' pattern of the moment history. The measured data also show a 'suction kick' at an actuator position of 4 ft that is not predicted by the model. However, bending moment measurements for subsequent load cycles show the absence of a suction kick. Hence, this particular discrepancy between prediction and measurement may be transitory and not necessarily relevant to long-term loading conditions. As noted above, work on validating and calibrating the seafloor-riser model presented has only recently been initiated, so the comparisons and observations presented are preliminary.

6 Conclusions

This paper presents a seafloor-riser interaction model based on an elastic pipe supported on nonlinear springs. Spring stiffness is described in terms of load-deflection (*P-y*) relationships that form a critical component of the model. The *P-y* model is formulated in terms of a backbone curve describing initial plastic penetration into the seafloor, a bounding loop describing load-deflection behavior under conditions of extreme deflection, and a series of rules for describing load-deflection behavior within the bounding loop. The *P-y* model is capable of modeling uplift and re-load cycles are conditions of partial and full detachment of the pipe from the seafloor. The soil-spring com-

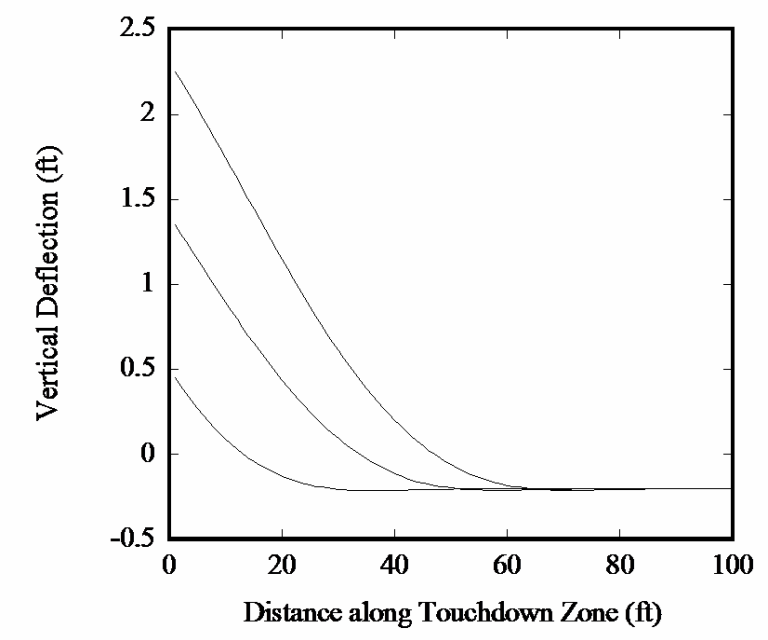

Figure 15: Example of riser deflected shapes obtained from the program.

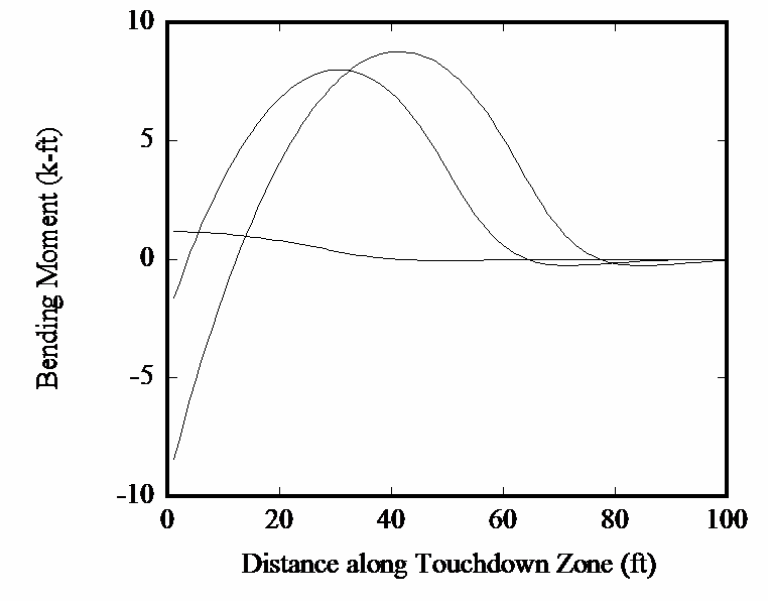

Figure 16: Example of predicted bending moment along the length of the riser

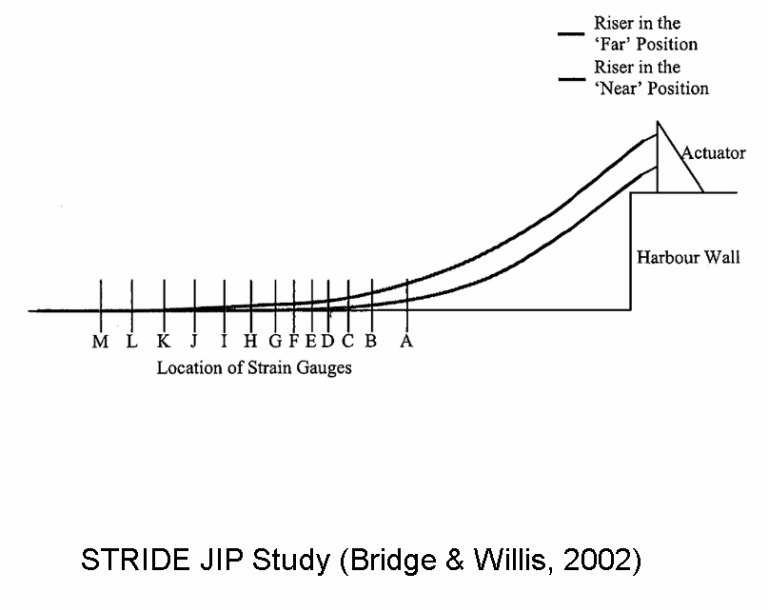

Figure 17: Schematic of the tests conducted by Bridge and Wiilis (2002)

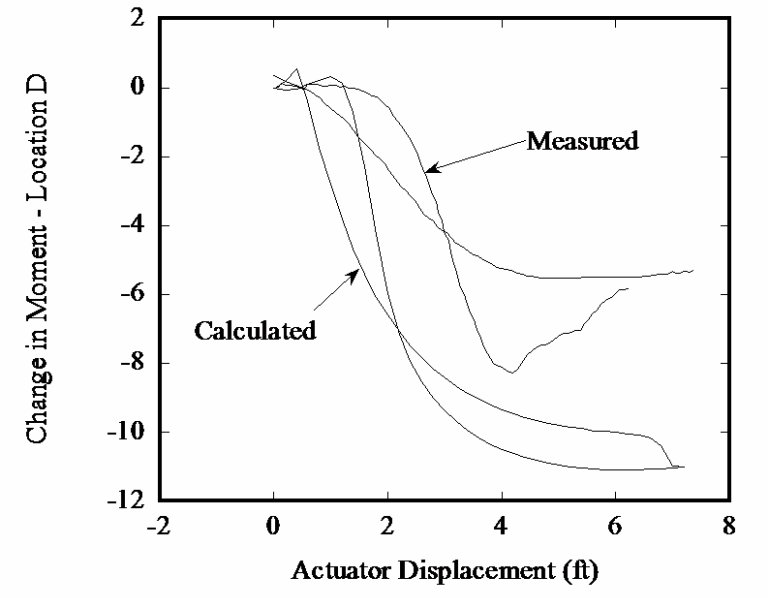

Figure 18: Comparison of estimated and measured moments at gauge D.

ponent of the model involves solution of a fourth-order, ordinary, non-linear differential equation. The computer code can be executed on a personal computer, and it was formulated with a view toward creating a design package readily accessible to designers.

The first component of the *P-y* model is a power law function (Eq. 5) to describe an initial penetration (backbone) curve. Laboratory model tests by Dunlap et al. (1990) and theoretical studies by Aubeny et al. (2005) support this form of the backbone curve function. *P-y* behavior during unloading and reloading from the backbone curve for conditions of large deflections is governed by a 'bounding loop'. The bounding loop can be defined in terms of three segments (Figure 3): elastic rebound from the backbone curve to the point at which maximum tension develops (Path 1-2), reduction in tension to the point of full separation between soil and pipe (Path 2-3), and soil-riser re-contact and re-loading (Path 3-1). The model describes the elastic rebound segment (Path 1-2) using a hyperbolic model, Eq. 13. Detailed evaluations of the Dunlap et al. (1990) data support the hyperbolic formulation. The model describes load Paths 2-3 and 3-1 in terms of cubic functions, Eqs. 14 and 17. Comparison of model simulations to data measurements (Figure 12) supports the adequacy of a cubic function for the case of Path 2-3. Review of additional test data is required to confirm its adequacy for the case of Path 3-1.

A general implementation of the model requires laws describing *P-y* behavior during load reversals from the bounding loop or within the bounding loop. The current form of the model presents rules for describing *P-y* behavior under these conditions, Eqs. 20 and 21. These rules have not yet been validated through comparison to laboratory test basin measurements; hence, the rules should be considered tentative until validation studies have been performed.

7 Ongoing and Future Work

This report presents a model for estimating fatigue stresses in a riser pipe for various conditions of vertical loading. Degradation of soil stiffness is recognized as a factor affecting fatigue life of a steel catenary riser. Incorporation of the stiffness degradation module is needed before the model can be implemented and the current model is being refined to account for this degradation. The experimental basis of the stiffness degradation component of the model will be measured load-displacement data on penetrating pipes. Since such data already exist, implementation of the model based on existing data is considered a realistic goal. Completion of this task is estimated by the end of 2006.

In addition, the model must be calibrated and validated through comparison to actual measurements. The calibration and validation of this model is the primary planned activity of the final phase of this research. Completion of this phase is estimated to be August 2007.

There is a plan, already in progress, to incorporate soil stiffness degradation into the model. In the OTRC research team view, since vertical motions are the more important factor governing fatigue life, the remaining research resources should be devoted to calibrating and validating the vertical motion model rather than attempting to model horizontal soil resistance. In our view, omitting lateral motions from consideration will not render the study immediately obsolete. The published literature indicate that a number of very large, cost intensive field and theoretical studies have been conducted with the primary, if not exclusive, focus being on vertical motions. These studies are frequently cited and by no means obsolete. The OTRC researchers feel that it is much more worthwhile to thoroughly understand and realistically model vertical interactions before proceeding to the less significant horizontal interactions.

ACKNOWLEDGEMENTS

The authors would also like to acknowledge the support of Department of the Interior Minerals Management Service (Cooperative Agreement No. 35515), the Offshore Technology Research Center and their colleagues at Texas A&M University.

BIBLIOGRAPHY

Aubeny, C. and Shi, H. (2006). "Interpretation of impact penetration measurements in soft clays." *J. Geotech. Geoenviron. Eng.*, 132(6), 770–777.

Aubeny, C., Shi, H., and Murff, J. (2005). "Collapse load for cylinder embedded in trench in cohesive soil." *International Journal of Geomechanics*, 5(4), 320–325.

Bridge, C., Howells, H., Toy, N., Parke, G., , and Woods, R. (2003). "Full-scale model tests of a steel catenary riser." *Fluid Structure Interaction II*, S. Chakrbarti, C. Brebbia, D. Almorza, and Gonzalez-Palma, eds., Southhampton, UK. WIT Press, 107–116.

Bridge, C., Laver, K., Clukey, E., and Evans, T. (2004). "Steel catenary riser touchdown point vertical interaction model,." *Offshore Technology Conference*, Houston, TX. OTC 16628.

Bridge, C. and Wiilis, N. (2002). "Steel catenary risers - results and conclusions from large scale simulations of seabed interaction." *Report no.*, DOT.

Bridge, C. and Willis, N. (2002). "Steel catenary risers - results and conclusions from large scale simulations of seafloor interactions." *Proceedings of the International Conference on Deep Offshore Technology*. Penn Well.

Clukey, E., Housterman s, L., and Dyvik, R. (2005). "Model tests to simulate riser-soil interaction effects in touchdown point region." *International Symposium on Frontiers in Offshore Geotechnics*, Perth, Australia. 651–658.

Dunlap, W., Bhohanala, R., and Morris, D. (1990). "Burial of vertically loaded offshore pipelines." *22nd Annual Offshore Technology Conference*, number OTC 6375, Houston, Texas. 263–270.

Hale, J., Morris, D., Yen, T., and Dunlap, W. (1992). "Modeling pipeline behavior on clay soils during storms." *24th Offshore Technology Conference*, number OTC 7019, Houston, TX. 339–349.

Hornbeck, R. (1975). *Numerical Methods*. Quantum Publishers, New Your, NY.

Morris, D., Webb, R., and Dunlap, W. (1988). "Self-burial of laterally loaded offshore pipelines." *20th Annual Offshore Technology Conference*, number OTC 5855, Houston, TX. 421–428.

Murff, J., Wagner, D., and Randolph, M. (1989). "Pipe penetration in cohesive soil." *Geotechnique*, 39(2), 213–229.

Pesce, C., Aranha, J., and Martins, C. (1998). "The soil rigidity effect in the touchdown boundary-layer of a catenary riser: static problem." *Proceedings of the Eighth International Offshore and Polar Engineering Conference*, International Society of Offshore and Polar Engineers, Montreal, Canada. 207.

Stewart, D. and Randolph, M. (1994). "T-bar penetration in soft clay." *Journal of Geotechnical Engineering, ASCE*, 118(12), 2230–2235.

Thethi, R. and Moros, T. (2001). "Soil interaction effects on simple catenary riser response." *Deepwater Pipeline & Riser Technology Conference*, Houston, TX.

Willis, N. and West, P. (2001). "Interaction between deepwater catenary risers and a soft seabed: large scale sea trials." *Offshore Technology Conference*, Houston, TX. OTC 13113.